

Topological and disorder corrections to the transverse Wiedemann-Franz law and Mott relation in kagome magnets and Dirac materials

Xiao-Bin Qiang ^{1,2,3,4} Z. Z. Du,^{1,3,4} Hai-Zhou Lu,^{1,2,3,4,*} and X. C. Xie^{5,6,7}

¹*Shenzhen Institute for Quantum Science and Engineering and Department of Physics, Southern University of Science and Technology (SUSTech), Shenzhen 518055, China*

²*Quantum Science Center of Guangdong-Hong Kong-Macao Greater Bay Area (Guangdong), Shenzhen 518045, China*

³*Shenzhen Key Laboratory of Quantum Science and Engineering, Shenzhen 518055, China*

⁴*International Quantum Academy, Shenzhen 518048, China*

⁵*International Center for Quantum Materials, School of Physics, Peking University, Beijing 100871, China*

⁶*Institute for Nanoelectronic Devices and Quantum Computing, Fudan University, Shanghai 200433, China*

⁷*Hefei National Laboratory, Hefei 230088, China*



(Received 25 September 2022; revised 9 April 2023; accepted 10 April 2023; published 26 April 2023; corrected 23 May 2023)

The Wiedemann-Franz law and Mott relation are textbook paradigms on the ratios of the thermal and thermoelectric conductivities to electrical conductivity, respectively. Deviations from them usually reveal insights for intriguing phases of matter. The recent topological kagome magnets TbMn_6Sn_6 and Mn_3Ge show confusingly opposite derivations in the Hall measurement. We calculate the topological and disorder corrections to the Wiedemann-Franz law and Mott relation for the Hall responses in topological kagome magnets and Dirac materials. The calculation indicates the dominance of the topological correction in the experiments. More importantly, we derive analytic correction formulas, which can universally capture the two opposite experiments with the chemical potential as the only parameter and will be a powerful guidance for future explorations on the magnetic topological matter and Dirac materials.

DOI: [10.1103/PhysRevB.107.L161302](https://doi.org/10.1103/PhysRevB.107.L161302)

In most metals, the ratio between the thermal conductivity κ and electric conductivity σ is characterized by the Wiedemann-Franz law $\kappa/\sigma = L_0 T$ [1], where T is the temperature and the Lorentz number

$$L_0 = (\pi k_B/e)^2/3 \quad (1)$$

is composed of the elementary charge e and the Boltzmann constant k_B . The deviations from them usually provide insights for exotic phases of matter, such as in non-Fermi liquids and hydrodynamics [2–11]. Recently, the thermoelectric and thermal transports have become promising tools to probe topological phases of matter [12–24]. In particular, topological magnets have attracted tremendous interest because of their outstanding electromagnetic conversion abilities for potential device applications [25–30]. The latest experiments on the topological kagome magnets TbMn_6Sn_6 [31] and Mn_3Ge [32] show confusingly opposite deviations from the Wiedemann-Franz law in the Hall measurements [Fig. 1(b)], raising questions on their microscopic mechanisms. In particular, disorder and topology could both play sophisticated roles in the anomalous Hall transport [33], but their contributions and competition remain unclear in these experiments.

In this Letter, we calculate the ratios of thermal Hall conductivity κ_{xy} and thermoelectric Hall (Nernst) conductivity α_{xy} to the electric Hall conductivity σ_{xy} [Fig. 1(a)]. Beyond

the previous works, we take into account the disorder contribution and topological contribution on the same footing. By comparing the calculation with the experiments, we find that the topological contribution may dominate in the experiments. More importantly, we can derive the analytic formulas for the corrections to the Wiedemann-Franz law (κ/σ) and Mott relation ($\alpha = -eL_0 T \partial\sigma/\partial\mu$, where μ is the chemical potential), with the help of the Dirac model that carry the topological and magnetic properties of the topological kagome magnets (Fig. 2). The analytic formulas depend not explicitly on the model details, but only on the chemical potential, implying the universal nature of the corrections. Our analytic formulas can reproduce both the negative and positive derivations from the classical Wiedemann-Franz law [Fig. 1(b)], as well as the tendencies in the Mott relation [Fig. 1(c)] in the experiments, with the same chemical potential in each experiment. These formulas will be helpful for further explorations on the electric, thermoelectric, and thermal transports in topological magnets and Dirac materials.

Despite the sophisticated magnetic structures of the topological kagome magnets, in the metallic phase as those in the experiments [31,32], the magnon [36–38] and phonon [1,39–43] degrees of freedom are inactive compared to electrons in the thermal Hall effect. Therefore, the electronic, thermoelectric, and thermal transports are fairly described by the electronic Hamiltonian. The electronic structure of TbMn_6Sn_6 can be described by the two-dimensional (2D) massive Dirac model, which has been confirmed by the spectroscopic measurement [30]. The electronic structure of the noncollinear

*Corresponding author: luhz@sustech.edu.cn

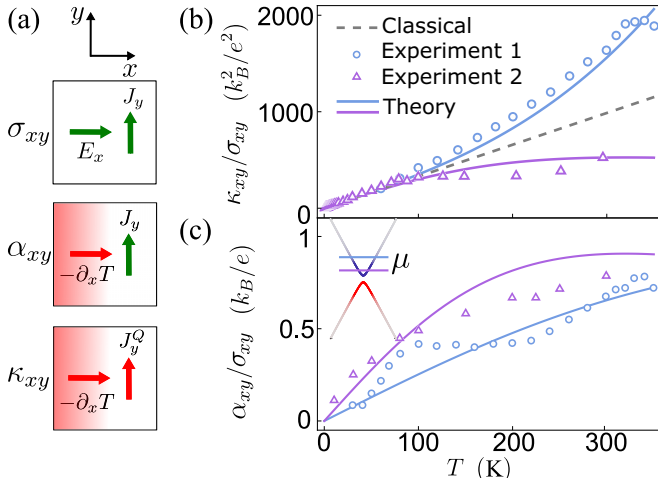


FIG. 1. (a) The electric Hall conductivity $\sigma_{xy} \equiv J_y/E_x$, thermoelectric Hall coefficient $\alpha_{xy} \equiv J_y/(-\partial_x T)$, and thermal Hall conductivity $\kappa_{xy} \equiv J_y^Q/(-\partial_x T)$, as the response of the transverse electric current J_y or thermal current J_y^Q to the longitudinal electric field E_x or temperature gradient $-\partial_x T$. Our analytical corrections (solid lines) to the classical behaviors (dashed lines) of (b) the ratios $\kappa_{xy}^{\text{in}}/\sigma_{xy}^{\text{in}}$ and (c) $\alpha_{xy}^{\text{in}}/\sigma_{xy}^{\text{in}}$ can capture two types of experiments (scatters), with the chemical potential μ as the only tuning parameter. We choose $\mu = 0.11$ and 0.05 eV for the TbMn_6Sn_6 [31] (Exp. 1) and Mn_3Ge [32] (Exp. 2) experiments, respectively. In the TbMn_6Sn_6 experiment, $\mu = 0.13$ eV.

antiferromagnet Mn_3Ge [Fig. 2(c)] [32] is the Weyl semimetal [35], which can be viewed as layers of coupled 2D massive Dirac models [44]. More importantly, the massive Dirac model can describe two of the most important characteristics of the topological kagome magnets, i.e., time-reversal symmetry breaking and topological properties. More importantly, later we will see that $\kappa_{xy}^{\text{in}}/\sigma_{xy}^{\text{in}}$ and $\alpha_{xy}^{\text{in}}/\sigma_{xy}^{\text{in}}$ in Eqs. (4) and (6) do not depend on the model details.

The electric, thermoelectric (Nernst coefficient), and thermal Hall conductivities can be expressed in an organized form

$$\sigma_{xy}^{\chi} = -\frac{e^2}{h} C_0^{\chi}, \quad \alpha_{xy}^{\chi} = \frac{k_B e}{h} C_1^{\chi}, \quad \kappa_{xy}^{\chi} = -\frac{k_B^2 T}{h} C_2^{\chi}, \quad (2)$$

where h is the Planck constant and the coefficient C_n^{χ} (see [45] for details) can be expressed as

$$C_n^{\chi} = \int d\varepsilon [\chi] \left(\frac{\varepsilon - \mu}{k_B T} \right)^n \left(-\frac{\partial f^0}{\partial \varepsilon} \right), \quad (3)$$

where ε is the energy, μ is the chemical potential, and $f^0 = 1/(e^{(\varepsilon - \mu)/k_B T} + 1)$ is the Fermi distribution function. The kernel function χ denotes different mechanisms in the anomalous transport, including the topological contribution revealed in the seminal works [12–14] and disorder contribution [46–48]. For the topological contribution, $\chi^{\text{in}} = 2\pi \sum_l \Omega_l^z f_l^0$, where $l = (\mathbf{k}, n)$ stands for the quantum numbers (momentum, band index), and Ω_l^z is the z component of the Berry curvature of band n with the definition $\Omega_l = i\nabla_{\mathbf{k}} \times \langle \psi_n | \nabla_{\mathbf{k}} \psi_n \rangle$. The Berry curvature can be understood as the “magnetic field” in the parameter space, as a result of the geometric structure of the quantum states [49], and is found

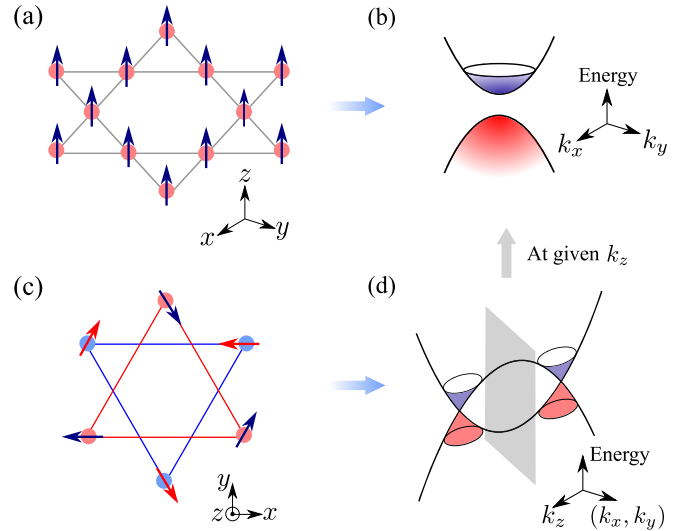


FIG. 2. Two typical topological kagome magnets. (a) TbMn_6Sn_6 with the out-of-plane magnetization [31] can be described by the 2D massive Dirac model (b), as verified by the fan diagram of the Landau levels under magnetic fields [30,34]. (c) The electronic behaviors of the layered (red for one sublayer, blue for the other) in-plane noncollinear antiferromagnet Mn_3Ge [32] is believed to be described by the Weyl semimetal [35], which can be viewed as layers of coupled 2D massive Dirac models (d).

critical in understanding the anomalous Hall effect [33,50], topological magnetoresistance [51–54], and thermal transport [12–14]. For the 2D Dirac model $\mathcal{H} = v(k_x \sigma_x + k_y \sigma_y) + m \sigma_z$, $\Omega_{\pm}^z = \mp m v^2 / (2\varepsilon_{\pm}^3)$, where the band dispersions are $\varepsilon_{\pm}(k) = \pm [v^2(k_x^2 + k_y^2) + m^2]^{1/2}$, v is the model parameter, $\sigma_{x,y,z}$ are Pauli matrices, and m is the band gap.

The main results of this work are the analytic formulas for the topological contributions $\kappa_{xy}^{\text{in}}/\sigma_{xy}^{\text{in}}$ (the Wiedemann-Franz law of the Hall signals) and $\alpha_{xy}^{\text{in}}/\sigma_{xy}^{\text{in}}$, which can reproduce two opposite types of experiments of the topological kagome magnets. By performing the Sommerfeld expansion of the transport coefficients [Eqs. (2)] with respect to the energy scale of temperature [up to $\sigma \propto (k_B T)^4$, $\alpha \propto (k_B T)^4$, $\kappa \propto (k_B T)^4$], we obtain the analytic expression for the ratio $\kappa_{xy}^{\text{in}}/\sigma_{xy}^{\text{in}}$,

$$\frac{\kappa_{xy}^{\text{in}}}{\sigma_{xy}^{\text{in}}} = \frac{15\mu^2/\pi^2 + 21(k_B T)^2}{15\mu^2/\pi^2 + 5(k_B T)^2 + 7\pi^2(k_B T)^4/\mu^2} L_0 T, \quad (4)$$

where the Lorentz number $L_0 = (\pi k_B/e)^2/3$, and the chemical potential μ is measured from the center of the gap. This formula can be simplified in two limits [45]:

$$\frac{\kappa_{xy}^{\text{in}}}{\sigma_{xy}^{\text{in}}} = \begin{cases} \left(1 + \frac{16\pi^2 k_B^2 T^2}{15 \mu^2}\right) L_0 T, & \mu \gg \mu_c \\ \left(1 + \frac{\pi^2 k_B^2 T^2}{3 \mu^2}\right)^{-1} L_0 T, & \mu \ll \mu_c, \end{cases} \quad (5)$$

where the critical chemical potential is found as $\mu_c = \sqrt{7}\pi k_B T/4$ (at which $\kappa_{xy}^{\text{in}}/\sigma_{xy}^{\text{in}}$ recovers the classical value $L_0 T$). The $\mu \gg \mu_c$ limit of Eq. (5) has been used to fit the positive deviation in the experiment of TbMn_6Sn_6 [31], but

only the new formula Eq. (4) can give both the positive and negative deviations in Fig. 1.

Similar to the classical Mott relation [1], we also get the relation between the thermoelectric and the electric Hall coefficients

$$\frac{\alpha_{xy}^{\text{in}}}{\sigma_{xy}^{\text{in}}} = \left(\frac{\mu}{e} + \frac{\pi^2 k_B^2 T^2}{3 e \mu} \right)^{-1} L_0 T. \quad (6)$$

Note that the formulas are independent of the model parameters but solely depend on μ , i.e., the position of the chemical potential. This is reasonable because the model details are canceled as the quantities on the denominator and numerator of the ratios both depend on the model parameters, such as the band gap m . In this sense, the ratios are more intrinsic and universal. Additionally, these formulas, i.e., Eqs. (4) and (6), can be generalized to other systems that can be well described by the 2D massive Dirac model, such as gapped 2D materials.

To test Eqs. (4) and (6), we use μ as the only parameter to fit the experimental data from Refs. [31,32]. Figures 1(b) and 1(c) show a good agreement between the experiments and our analytic formulas for $\kappa_{xy}^{\text{in}}/\sigma_{xy}^{\text{in}}$ and $\alpha_{xy}^{\text{in}}/\sigma_{xy}^{\text{in}}$ as functions of temperature T . In particular, we use $\mu = 0.11$ eV to fit the data of TbMn₆Sn₆, very close to the measured $\mu = 0.13 \pm 0.004$ eV in the experiment [30]. We stress that the fitting parameter μ is the same for $\kappa_{xy}^{\text{in}}/\sigma_{xy}^{\text{in}}$ and $\alpha_{xy}^{\text{in}}/\sigma_{xy}^{\text{in}}$ for the same experiment in the comparison. Constrained by the Sommerfeld expansion, our formulas in Eqs. (4) and (6) are valid for temperatures below the Fermi temperature $T_F = \mu/k_B$, which is more than 1000 K for the high chemical potentials in the experiments. Nevertheless, there is a derivation from the formula above 300 K.

It is reasonable to employ the formulas, because the electronic behaviors of the topological kagome magnet TbMn₆Sn₆ [30,31,34] and the noncollinear antiferromagnet Mn₃Ge [32,35] can be reduced to the 2D massive Dirac model (Fig. 2). The description of Mn₃Ge by the 2D model is further supported by considering a three-dimensional (3D) tilted massless Weyl cone [55,56] $\mathcal{H} = s(v\mathbf{k} \cdot \boldsymbol{\sigma} + tk_z)$, where v is the model parameter, and $s = \pm 1$ labels the chirality of a single node. The tilt term tk_z is necessary to cover a more general case, and we assume $t/v \ll 1$ to get the analytical result. This model can well describe the Weyl semimetal phase in the bulk Mn₃Ge [56]. We find that there is no deviation from the Wiedemann-Franz law and Mott relation when both the topology and disorder contributions are taken into account for the tilted massless Weyl cone (details can be found in [45]), additionally justifying that the 2D model is a better description for the layered structure of Mn₃Ge.

Up to now, we only consider the topological correction. However, disorder in real materials can contribute to the anomalous transport [33,46–48,57]. We use the Boltzmann kinetics to account for the disorder contribution, which is widely used in explaining magnetotransport [54,58–60] and nonlinear transport [61–65]. To have analytic results, we consider a δ -correlated disorder model $\hat{V}_{\text{imp}} = \sum_i V_i \delta(\mathbf{r} - \mathbf{R}_i)$ with the randomly distributed vector R_i and the disorder strength V_i satisfying the second-order correlation $\langle V_i^2 \rangle_{\text{dis}} = V_0^2$ and third-order correlation $\langle V_i^3 \rangle_{\text{dis}} = V_1^3$. This model can well describe the elastic scattering (even the electron-phonon

scattering approximately below the Debye temperature [1]). After a lengthy calculation [45], we find the kernel functions for the disorder contributions, including the side-jump, extrinsic skew-scattering, and intrinsic skew-scattering parts, respectively,

$$\begin{aligned} \chi^{sj} &= \frac{2m(\varepsilon^2 - m^2)}{\varepsilon(\varepsilon^2 + 3m^2)}, \\ \chi^{sk,1} &= \frac{V_1^3 m(\varepsilon^2 - m^2)^2}{n_i V_0^4 (\varepsilon^2 + 3m^2)^2}, \\ \chi^{sk,2} &= \frac{3m(\varepsilon^2 - m^2)^2}{2\varepsilon(\varepsilon^2 + 3m^2)^2}. \end{aligned} \quad (7)$$

By substituting χ 's into Eq. (3), we can have the total contribution that includes the topological and disorder contributions for all transport coefficients, as well as the ratios $\kappa_{xy}^{\text{tot}}/\sigma_{xy}^{\text{tot}}$ and $\alpha_{xy}^{\text{tot}}/\sigma_{xy}^{\text{tot}}$.

Interestingly, in the presence of the disorder contribution, up to the leading-order [$\sigma \propto (k_B T)^0$, $\alpha \propto (k_B T)^2$, $\kappa \propto (k_B T)^2$] Sommerfeld expansion of Eq. (3), the ratios can recover the classical Wiedemann-Franz law and Mott relation, i.e. (check [45] for details),

$$\begin{aligned} \kappa_{xy}^{\text{in}(0)} + \kappa_{xy}^{\text{dis}(0)} &= L_0 T [\sigma_{xy}^{\text{in}(0)} + \sigma_{xy}^{\text{dis}(0)}], \\ \alpha_{xy}^{\text{in}(0)} + \alpha_{xy}^{\text{dis}(0)} &= -e L_0 T \frac{\partial}{\partial \mu} [\sigma_{xy}^{\text{in}(0)} + \sigma_{xy}^{\text{dis}(0)}], \end{aligned} \quad (8)$$

where the superscript (0) means leading order and *dis*(0) includes the leading-order side-jump and skew-scattering contributions.

To fully examine the disorder correction, we numerically evaluate $\kappa_{xy}^{\text{tot}}/\sigma_{xy}^{\text{tot}}$ and $\alpha_{xy}^{\text{tot}}/\sigma_{xy}^{\text{tot}}$ by using Eqs. (3) and (7) for different values of m and μ . As shown in Figs. 3(a) and 3(b), both $\kappa_{xy}^{\text{tot}}/\sigma_{xy}^{\text{tot}}$ and $\alpha_{xy}^{\text{tot}}/\sigma_{xy}^{\text{tot}}$ show the m dependence, which is different when there is only the topological contribution. We adopt the value $m = 0.017$ eV for TbMn₆Sn₆ [31], i.e., black curves in [Figs. 3(c) and 3(d)]. It can be seen that the topological and total contributions show different behaviors. For κ_{xy}/σ_{xy} , the total contribution shows almost only negative correction to the Wiedemann-Franz law, unable to describe the positive deviation in the TbMn₆Sn₆ experiment [31]. Similarly, if we include the disorder contribution, the total correction to α_{xy}/σ_{xy} is also not consistent with the experiment [31]. These results imply that the topological contribution is dominant in these topological kagome magnet experiments so far [31,32].

To see if the above results based on the 2D Dirac model can be generalized to 3D, we also use a 3D Dirac model to calculate the topological correction to $\kappa_{xy}^{\text{in}}/\sigma_{xy}^{\text{in}}$ and $\alpha_{xy}^{\text{in}}/\sigma_{xy}^{\text{in}}$ [67–69],

$$\mathcal{H} = v\mathbf{k} \cdot \boldsymbol{\alpha} + (m - bk^2)\beta + M\sigma_0 \otimes \sigma_z, \quad (9)$$

where v , m , b , and M are model parameters, $\alpha_i = \sigma_x \otimes \sigma_i$ and $\beta = \sigma_z \otimes \sigma_0$ are Dirac matrices, and $\mathbf{k} = (k_x, k_y, k_z)$ is the wave vector with $k = |\mathbf{k}|$. When the parameters $mb > 0$, this model can characterize a magnetic topological insulator. The last term is the Zeeman energy that describes magnetism,

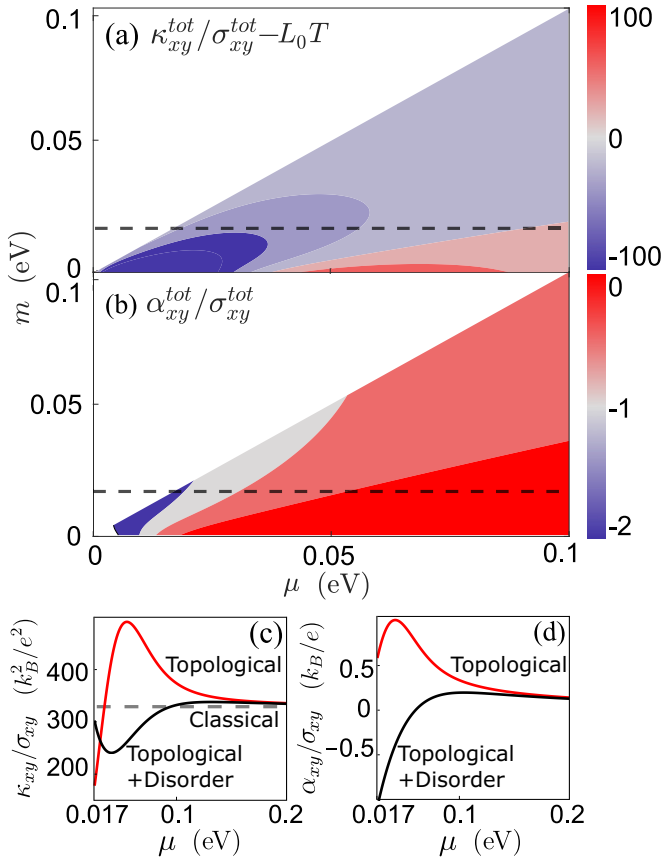


FIG. 3. (a) The total (topological + disorder) contribution to the deviation of the Wiedemann-Franz law $\kappa_{xy}^{tot}/\sigma_{xy}^{tot} - L_0 T$ in units of k_B^2/e^2 , and (b) $\alpha_{xy}^{tot}/\sigma_{xy}^{tot}$ in units of k_B/e for the 2D massive Dirac model. The dashed lines represent $m = 0.017$ eV for the TbMn₆Sn₆ [31]. (c),(d) The chemical potential μ dependence of two ratios for the topological (red) and total (black) contributions with $m = 0.017$ eV. The parameters are $v = 1$ eV nm, $n_i V_0^4/V_1^3 = 1$ eV, and $T = 100$ K.

which breaks time-reversal symmetry to unveil the hidden Berry curvature, as seen in the inset of Fig. 4(d).

In Fig. 4, we present the numerical results of $\kappa_{xy}^{in}/\sigma_{xy}^{in}$ and $\alpha_{xy}^{in}/\sigma_{xy}^{in}$ for the 3D Dirac model in Eq. (9), which show similar temperature and chemical potential dependencies to those described by the 2D Dirac model and in the experiments. Specifically, the violation of the classical Wiedemann-Franz law becomes stronger as the chemical potential approaches the band edge and as temperature is increased, and $\kappa_{xy}^{in}/\sigma_{xy}^{in}$ is below and above the classical value, respectively, as the chemical potential is very close to and moves away from the band edge. These numerical results of the 3D Dirac model show that our analytical formulas based on the 2D Dirac model could be a qualitative tool to study the topological corrections to the Wiedemann-Franz law and Mott relation in the topological magnets and Dirac materials.

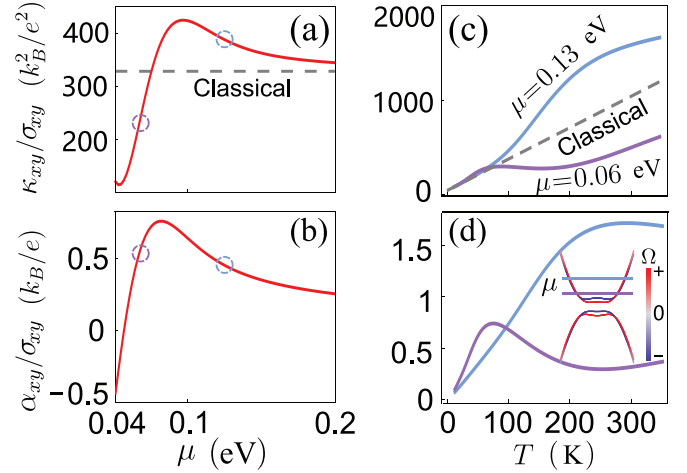


FIG. 4. (a),(b) For the 3D Dirac model [Eq. (9)], $\kappa_{xy}^{in}/\sigma_{xy}^{in}$ (a) and $\alpha_{xy}^{in}/\sigma_{xy}^{in}$ (b) as functions of the chemical potential μ at 100 K. The dashed lines represent the classical Wiedemann-Franz law. The purple and blue circles indicate $\mu = 0.06$ eV and $\mu = 0.13$ eV, corresponding to the two curves in (c) and (d). (c),(d) $\kappa_{xy}^{in}/\sigma_{xy}^{in}$ (c) and $\alpha_{xy}^{in}/\sigma_{xy}^{in}$ (d) as functions of temperature T , for $\mu = 0.06$ eV and $\mu = 0.13$ eV (the solid curves). Inset of (d) depicts the dispersion and Berry curvature Ω of the energy bands for the 3D Dirac model with the Zeeman energy, which lifts the degeneracy of the bands. The parameters are $v = 0.1$ eV nm, $m = -0.04$ eV, $b = -0.18$ eV nm², and $M = 5.788 \times 10^{-3}$ eV [66].

To conclude, we analytically and numerically calculated the corrections to the Wiedemann-Franz law and Mott relation for topological kagome magnets and Dirac materials, by treating the topological correction and disorder correction on the same footing. By comparing our results with the recent experiments with opposite behaviors, we show the dominance of the topological correction from the Berry curvature in the experiments. More importantly, our analytic formulas for the topological correction will be a useful tool to explore the emergent topological magnets and Dirac materials.

We thank J.-X. Yin for helpful discussions. This work was supported by the National Key R&D Program of China (Grant No. 2022YFA1403700), the Innovation Program for Quantum Science and Technology (Grant No. 2021ZD0302400), the National Natural Science Foundation of China (Grant No. 11925402), Guangdong province (Grants No. 2020KCXTD001 and No. 2016ZT06D348), the Science, Technology and Innovation Commission of Shenzhen Municipality (Grants No. ZDSYS20170303165926217, No. JAY20170412152620376, and No. KYTDPT20181011104202253). The numerical calculations were supported by Center for Computational Science and Engineering of SUSTech.

- [1] N. W. Ashcroft and N. D. Mermin, *Solid State Physics* (Cengage Learning, 2022).
- [2] R. Mahajan, M. Barkeshli, and S. A. Hartnoll, Non-Fermi liquids and the Wiedemann-Franz law, *Phys. Rev. B* **88**, 125107 (2013).

- [3] A. Lavasani, D. Bulmash, and S. Das Sarma, Wiedemann-Franz law and Fermi liquids, *Phys. Rev. B* **99**, 085104 (2019).
- [4] B. Kubala, J. König, and J. Pekola, Violation of the Wiedemann-Franz Law in a Single-Electron Transistor, *Phys. Rev. Lett.* **100**, 066801 (2008).

- [5] A. Principi and G. Vignale, Violation of the Wiedemann-Franz Law in Hydrodynamic Electron Liquids, *Phys. Rev. Lett.* **115**, 056603 (2015).
- [6] C. Xiao, D. Li, and Z. Ma, Unconventional thermoelectric behaviors and enhancement of figure of merit in Rashba spintronic systems, *Phys. Rev. B* **93**, 075150 (2016).
- [7] A. Lucas and S. Das Sarma, Electronic hydrodynamics and the breakdown of the Wiedemann-Franz and Mott laws in interacting metals, *Phys. Rev. B* **97**, 245128 (2018).
- [8] K.-S. Kim and C. Pépin, Violation of the Wiedemann-Franz Law at the Kondo Breakdown Quantum Critical Point, *Phys. Rev. Lett.* **102**, 156404 (2009).
- [9] F. Bucceri, A. Nava, R. Egger, P. Sodano, and D. Giuliano, Violation of the Wiedemann-Franz law in the topological Kondo model, *Phys. Rev. B* **105**, L081403 (2022).
- [10] Z. Wang, R. Boyack, and K. Levin, Heat-bath approach to anomalous thermal transport: Effects of inelastic scattering, *Phys. Rev. B* **105**, 134302 (2022).
- [11] T. Nag and S. Nandy, Magneto-transport phenomena of type-I multi-Weyl semimetals in co-planar setups, *J. Phys.: Condens. Matter* **33**, 075504 (2020).
- [12] D. Xiao, Y. Yao, Z. Fang, and Q. Niu, Berry-Phase Effect in Anomalous Thermoelectric Transport, *Phys. Rev. Lett.* **97**, 026603 (2006).
- [13] D. L. Bergman and V. Oganesyan, Theory of Dissipationless Nernst Effects, *Phys. Rev. Lett.* **104**, 066601 (2010).
- [14] T. Yokoyama and S. Murakami, Transverse magnetic heat transport on the surface of a topological insulator, *Phys. Rev. B* **83**, 161407(R) (2011).
- [15] C. T. Bui and F. Rivadulla, Anomalous and planar Nernst effects in thin films of the half-metallic ferromagnet $\text{La}_{2/3}\text{Sr}_{1/3}\text{MnO}_3$, *Phys. Rev. B* **90**, 100403(R) (2014).
- [16] M. Hirschberger, S. Kushwaha, Z. Wang, Q. Gibson, S. Liang, C. A. Belvin, B. A. Bernevig, R. J. Cava, and N. P. Ong, The chiral anomaly and thermopower of Weyl fermions in the half-Heusler GdPtBi , *Nat. Mater.* **15**, 1161 (2016).
- [17] G. Sharma, P. Goswami, and S. Tewari, Nernst and magnetothermal conductivity in a lattice model of Weyl fermions, *Phys. Rev. B* **93**, 035116 (2016).
- [18] J. Noky, J. Gayles, C. Felser, and Y. Sun, Strong anomalous Nernst effect in collinear magnetic Weyl semimetals without net magnetic moments, *Phys. Rev. B* **97**, 220405(R) (2018).
- [19] S. Nandy, A. Taraphder, and S. Tewari, Planar thermal Hall effect in Weyl semimetals, *Phys. Rev. B* **100**, 115139 (2019).
- [20] J. L. Zhang, C. M. Wang, C. Y. Guo, X. D. Zhu, Y. Zhang, J. Y. Yang, Y. Q. Wang, Z. Qu, L. Pi, H.-Z. Lu, and M. L. Tian, Anomalous Thermoelectric Effects of ZrTe_5 in and beyond the Quantum Limit, *Phys. Rev. Lett.* **123**, 196602 (2019).
- [21] C. Zeng, S. Nandy, and S. Tewari, Chiral anomaly induced nonlinear Nernst and thermal Hall effects in Weyl semimetals, *Phys. Rev. B* **105**, 125131 (2022).
- [22] C. Fu, Y. Sun, and C. Felser, Topological thermoelectrics, *APL Mater.* **8**, 040913 (2020).
- [23] S. Minami, F. Ishii, M. Hirayama, T. Nomoto, T. Koretsune, and R. Arita, Enhancement of the transverse thermoelectric conductivity originating from stationary points in nodal lines, *Phys. Rev. B* **102**, 205128 (2020).
- [24] P. Wang, C.-w. Cho, F. Tang, P. Wang, W. Zhang, M. He, G. Gu, X. Wu, Y. Shao, and L. Zhang, Giant Nernst effect and field-enhanced transversal $z_n T$ in ZrTe_5 , *Phys. Rev. B* **103**, 045203 (2021).
- [25] S. Nakatsuji, N. Kiyohara, and T. Higo, Large anomalous Hall effect in a non-collinear antiferromagnet at room temperature, *Nature (London)* **527**, 212 (2015).
- [26] Z. Lin, J.-H. Choi, Q. Zhang, W. Qin, S. Yi, P. Wang, L. Li, Y. Wang, H. Zhang, Z. Sun *et al.*, Flatbands and Emergent Ferromagnetic Ordering in Fe_3Sn_2 Kagome Lattices, *Phys. Rev. Lett.* **121**, 096401 (2018).
- [27] L. Ye, M. Kang, J. Liu, F. Von Cube, C. R. Wicker, T. Suzuki, C. Jozwiak, A. Bostwick, E. Rotenberg, D. C. Bell *et al.*, Massive Dirac fermions in a ferromagnetic kagome metal, *Nature (London)* **555**, 638 (2018).
- [28] J.-X. Yin, S. S. Zhang, H. Li, K. Jiang, G. Chang, B. Zhang, B. Lian, C. Xiang, I. Belopolski, H. Zheng *et al.*, Giant and anisotropic many-body spin-orbit tunability in a strongly correlated kagome magnet, *Nature (London)* **562**, 91 (2018).
- [29] J.-X. Yin, S. S. Zhang, G. Chang, Q. Wang, S. S. Tsirkin, Z. Guguchia, B. Lian, H. Zhou, K. Jiang, I. Belopolski *et al.*, Negative flat band magnetism in a spin-orbit-coupled correlated kagome magnet, *Nat. Phys.* **15**, 443 (2019).
- [30] J.-X. Yin, W. Ma, T. A. Cochran, X. Xu, S. S. Zhang, H.-J. Tien, N. Shumiya, G. Cheng, K. Jiang, B. Lian *et al.*, Quantum-limit Chern topological magnetism in TbMn_6Sn_6 , *Nature (London)* **583**, 533 (2020).
- [31] X. Xu, J.-X. Yin, W. Ma, H.-J. Tien, X.-B. Qiang, P. Reddy, H. Zhou, J. Shen, H.-Z. Lu, T.-R. Chang *et al.*, Topological charge-entropy scaling in kagome Chern magnet TbMn_6Sn_6 , *Nat. Commun.* **13**, 1197 (2022).
- [32] L. Xu, X. Li, X. Lu, C. Collignon, H. Fu, J. Koo, B. Fauqué, B. Yan, Z. Zhu, and K. Behnia, Finite-temperature violation of the anomalous transverse Wiedemann-Franz law, *Sci. Adv.* **6**, eaaz3522 (2020).
- [33] N. Nagaosa, J. Sinova, S. Onoda, A. H. MacDonald, and N. P. Ong, Anomalous Hall effect, *Rev. Mod. Phys.* **82**, 1539 (2010).
- [34] G. Xu, B. Lian, and S.-C. Zhang, Intrinsic Quantum Anomalous Hall Effect in the Kagome Lattice $\text{Cs}_2\text{LiMnF}_{12}$, *Phys. Rev. Lett.* **115**, 186802 (2015).
- [35] J. Kübler and C. Felser, Non-collinear antiferromagnets and the anomalous Hall effect, *Europhys. Lett.* **108**, 67001 (2014).
- [36] Y. Onose, T. Ideue, H. Katsura, Y. Shiomi, N. Nagaosa, and Y. Tokura, Observation of the magnon Hall effect, *Science* **329**, 297 (2010).
- [37] T. Ideue, Y. Onose, H. Katsura, Y. Shiomi, S. Ishiwata, N. Nagaosa, and Y. Tokura, Effect of lattice geometry on magnon Hall effect in ferromagnetic insulators, *Phys. Rev. B* **85**, 134411 (2012).
- [38] R. R. Neumann, A. Mook, J. Henk, and I. Mertig, Thermal Hall Effect of Magnons in Collinear Antiferromagnetic Insulators: Signatures of Magnetic and Topological Phase Transitions, *Phys. Rev. Lett.* **128**, 117201 (2022).
- [39] J. M. Ziman, *Electrons and Phonons: The Theory of Transport Phenomena in Solids* (Oxford University Press, New York, 2001).
- [40] C. Strohm, G. L. J. A. Rikken, and P. Wyder, Phenomenological Evidence for the Phonon Hall Effect, *Phys. Rev. Lett.* **95**, 155901 (2005).
- [41] J.-S. Wang and L. Zhang, Phonon Hall thermal conductivity from the Green-Kubo formula, *Phys. Rev. B* **80**, 012301 (2009).

- [42] L. Zhang, J. Ren, J.-S. Wang, and B. Li, Topological Nature of the Phonon Hall Effect, *Phys. Rev. Lett.* **105**, 225901 (2010).
- [43] K. Sun, Z. Gao, and J.-S. Wang, Phonon Hall effect with first-principles calculations, *Phys. Rev. B* **103**, 214301 (2021).
- [44] A. A. Burkov and L. Balents, Weyl Semimetal in a Topological Insulator Multilayer, *Phys. Rev. Lett.* **107**, 127205 (2011).
- [45] See Supplemental Material at <http://link.aps.org/supplemental/10.1103/PhysRevB.107.L161302> for (Sec. SI) Boltzmann kinetics, (Sec. SII) anomalous electric Hall effect, (Sec. SIII) anomalous thermoelectric Hall effect, (Sec. SIV) anomalous thermal Hall effect, (Sec. SV) 2-band system, (Sec. SVI) 2D massive Dirac model, and (Sec. SVII) tilted Weyl node, which includes Refs. [33,47,48].
- [46] N. A. Sinitsyn, J. E. Hill, H. Min, J. Sinova, and A. H. MacDonald, Charge and Spin Hall Conductivity in Metallic Graphene, *Phys. Rev. Lett.* **97**, 106804 (2006).
- [47] N. A. Sinitsyn, A. H. MacDonald, T. Jungwirth, V. K. Dugaev, and J. Sinova, Anomalous Hall effect in a two-dimensional Dirac band: The link between the Kubo-Streda formula and the semiclassical Boltzmann equation approach, *Phys. Rev. B* **75**, 045315 (2007).
- [48] M. Papaj and L. Fu, Enhanced anomalous Nernst effect in disordered Dirac and Weyl materials, *Phys. Rev. B* **103**, 075424 (2021).
- [49] M. V. Berry, Quantal phase factors accompanying adiabatic changes, *Proc. R. Soc. London A* **392**, 45 (1984).
- [50] D. Xiao, M.-C. Chang, and Q. Niu, Berry phase effects on electronic properties, *Rev. Mod. Phys.* **82**, 1959 (2010).
- [51] D. T. Son and B. Z. Spivak, Chiral anomaly and classical negative magnetoresistance of Weyl metals, *Phys. Rev. B* **88**, 104412 (2013).
- [52] A. A. Burkov, Chiral Anomaly and Diffusive Magnetotransport in Weyl Metals, *Phys. Rev. Lett.* **113**, 247203 (2014).
- [53] Y. Pan, H. Wang, P. Lu, J. Sun, B. Wang, and D. Xing, The large unsaturated magnetoresistance of Weyl semimetals, [arXiv:1509.03975](https://arxiv.org/abs/1509.03975).
- [54] X. Dai, Z. Z. Du, and H.-Z. Lu, Negative Magnetoresistance without Chiral Anomaly in Topological Insulators, *Phys. Rev. Lett.* **119**, 166601 (2017).
- [55] D. Ma, H. Jiang, H. Liu, and X. C. Xie, Planar Hall effect in tilted Weyl semimetals, *Phys. Rev. B* **99**, 115121 (2019).
- [56] G. Chaudhary, A. A. Burkov, and O. G. Heinonen, Magnetism and magnetotransport in the kagome antiferromagnet Mn_3Ge , *Phys. Rev. B* **105**, 085108 (2022).
- [57] H.-Z. Lu and S.-Q. Shen, Extrinsic anomalous Hall conductivity of a topologically nontrivial conduction band, *Phys. Rev. B* **88**, 081304(R) (2013).
- [58] S.-K. Yip, Kinetic equation and magneto-conductance for Weyl metal in the clean limit, [arXiv:1508.01010](https://arxiv.org/abs/1508.01010).
- [59] B. Z. Spivak and A. V. Andreev, Magnetotransport phenomena related to the chiral anomaly in Weyl semimetals, *Phys. Rev. B* **93**, 085107 (2016).
- [60] A. V. Andreev and B. Z. Spivak, Longitudinal Negative Magnetoresistance and Magnetotransport Phenomena in Conventional and Topological Conductors, *Phys. Rev. Lett.* **120**, 026601 (2018).
- [61] I. Sodemann and L. Fu, Quantum Nonlinear Hall Effect Induced by Berry Curvature Dipole in Time-Reversal Invariant Materials, *Phys. Rev. Lett.* **115**, 216806 (2015).
- [62] Z. Z. Du, C. M. Wang, H.-Z. Lu, and X. C. Xie, Band Signatures for Strong Nonlinear Hall Effect in Bilayer WTe_2 , *Phys. Rev. Lett.* **121**, 266601 (2018).
- [63] Z. Z. Du, C. Wang, S. Li, H.-Z. Lu, and X. Xie, Disorder-induced nonlinear Hall effect with time-reversal symmetry, *Nat. Commun.* **10**, 3047 (2019).
- [64] Z. Z. Du, H.-Z. Lu, and X. C. Xie, Nonlinear Hall effects, *Nat. Rev. Phys.* **3**, 744 (2021).
- [65] D.-K. Zhou, Z.-F. Zhang, X.-Q. Yu, Z.-G. Zhu, and G. Su, Fundamental distinction between intrinsic and extrinsic nonlinear thermal Hall effects, *Phys. Rev. B* **105**, L201103 (2022).
- [66] B. Fu, H.-W. Wang, and S.-Q. Shen, Quantum Interference Theory of Magnetoresistance in Dirac Materials, *Phys. Rev. Lett.* **122**, 246601 (2019).
- [67] S.-Q. Shen, *Topological Insulators: Dirac Equation in Condensed Matter* (Springer, New York, 2017).
- [68] F. Qin, S. Li, Z. Z. Du, C. M. Wang, W. Zhang, D. Yu, H.-Z. Lu, and X. C. Xie, Theory for the Charge-Density-Wave Mechanism of 3D Quantum Hall Effect, *Phys. Rev. Lett.* **125**, 206601 (2020).
- [69] R. Chen, H.-P. Sun, and B. Zhou, Side-surface-mediated hybridization in axion insulators, *Phys. Rev. B* **107**, 125304 (2023).

Correction: A typographical error in first grant number in the Acknowledgments has been fixed.